Egyptian Journal of Radiology and Nuclear Medicine

RESEARCH Open Access

Phase-contrast magnetic resonance imaging in evaluation of hydrocephalus in pediatric patients

Gehad Ahmed El-Sayed Sakr[1], Manal Fathy Hamisa[1,2], Yasser Fouad El Sawaf[1,3] and Hanan Ahmad Nagy[2*]

Abstract

Background Hydrocephalus is an increase in cerebrospinal fluid volume leading to cerebral ventricular enlargement (ventriculomegaly). Phase-contrast magnetic resonance imaging is a sensitive technique to cerebrospinal fluid flow allowing noninvasive quantitative and qualitative evaluation of cerebrospinal fluid flow.

Aim The purpose of our study was to assess the role of cerebrospinal fluid flowmetry using phase-contrast magnetic resonance imaging in evaluation of hydrocephalus in pediatric patients.

Methods This prospective study included a group of 50 patients with ventriculomegaly diagnosed by a previous magnetic resonance imaging study. A control group of 20 subjects of matched age group were also included. All the participants were subjected to cerebrospinal fluid flow study.

Results After quantitative assessment of cerebrospinal fluid flow at aqueduct level, the mean values of flow and velocity parameters were compared in both patients and control groups. The mean values in patients with aqueduct stenosis and Dandy–Walker malformation were significantly lower than those of the control group (no flow with hypodynamic circulation) with $p < 0.001, < 0.017$ for mean velocity, respectively, the mean values in patients with brain atrophy and Arnold–Chiari malformation, bilateral obstructive hydrocephalus at foramen of Monro were significantly lower than those of the control group (diminished flow with hypodynamic circulation) with $p < 0.001, < 0.001, 0.046$ for mean velocity, respectively, and 0.002, 0.001, 0.160 for stroke volume, respectively, the mean values in patients with communicating hydrocephalus and unilateral obstructive hydrocephalus at foramen of Monro were significantly higher than those of the control group (hyperdynamic flow) with $p < 0.001$ for mean velocity and stroke volume, and the mean values in patients with arachnoid cysts were within normal as compared to control group (normal dynamic flow).

Conclusion Phase-contrast magnetic resonance imaging is a noninvasive technicality used for evaluation of cerebrospinal fluid flow both qualitatively and quantitatively for determining the type of hydrocephalus seen.

Keywords CSF flowmetry, Hydrocephalus, Phase-contrast MRI, Pediatric

Background

The choroid plexus of lateral ventricles are responsible for formation of most of the cerebrospinal fluid (CSF). The rate of formation in pediatric and adult population is 0.35–0.40 ml/min equivalent to 500 ml per day [1].

Hydrocephalus means an excess fluid accumulation in the brain due to dynamic imbalance between

*Correspondence:
Hanan Ahmad Nagy
hanan.nagy84@hotmail.com
[1] Ministry of Health, El-Geish Street, Tanta, Gharbya Governorate, Egypt
[2] Radiodiagnosis and Medical Imagining, Faculty of Medicine, Tanta University, El-Geish Street, Tanta, Gharbya Governorate, Egypt
[3] Faculty of Medicine, Tanta University, El-Geish Street, Tanta, Gharbya Governorate, Egypt

cerebrospinal fluid (CSF) production and absorption causing enlarged ventricles [1, 2].

Non-communicating or obstructive hydrocephalus is a type with obstructed CSF flow from the ventricles to subarachnoid space with no communication between them. The commonest cause of this type is aqueduct obstruction [1].

While in communicating or non-obstructive hydrocephalus, CSF flow is not obstructed, but inadequately reabsorbed in the subarachnoid space with preserved communication between the ventricular system and the subarachnoid space. The commonest cause of this group is post-infective and post-hemorrhagic hydrocephalus [1].

The cerebrospinal fluid circulation in the brain is complex and needs much more understanding of CSF abnormalities that can be causes or markers of diseases [3].

So, phase-contrast magnetic resonant imaging (MRI) is an emerging technique that facilitates imaging of CSF flow dynamic and allows quantitative and qualitative evaluation of CSF flow at key anatomic sites, such as the cerebral aqueduct of Sylvius and the foramen magnum [3].

PCMRI is a simple, prompt, and noninvasive technique with an acceptable sensitivity to little CSF flows; Cine PC-MR images display CSF flow in a dynamic, readily, and considerable mode differentiating between communicating and non-communicating hydrocephalus, allowing better recognition of obstruction, if present, in the most common sites of obstruction along CSF pathway as foramen of Monro, and aqueduct of Sylvius, assessment of arachnoid cysts, and recognition of CSF movements in Chiari and Dandy–walker malformations [4–6].

Measurement of CSF flow at a suspicious obstruction level affords dependable outcome for an exact diagnosis, detection of a combination of pathologies, better placement of method of treatment, and improving the postoperative outcome [4, 7].

The aim of this study is to evaluate CSF dynamic by CSF flowmetry using phase-contrast magnetic resonance imaging for more accurate diagnosis of different types of hydrocephalus in children.

Methods

Study population

The current prospective study included 50 patients having ventriculomegaly diagnosed by a previous MRI study; their ages ranged from 1 to 12 years with a mean of 5.080 ± 3.303 years. They were referred to MRI unit in Radio-diagnosis department from neurosurgery department over a period from February 2019 to February 2021. A control group of 20 individual were also included. Both groups correspond in terms of age and sex to avert bias.

Approval of Research Ethics Committee (REC) and informed consent were obtained from parents after explanation of the benefits and risks of the procedure. Privacy and confidentiality of all patients' data were guaranteed. All data provision was monitored and used for scientific purpose only.

The inclusion criteria of patients and controls were: subjects within pediatric age group, up to 18 years, and no gender predilection. According to patients, they were diagnosed with ventriculomegaly by a previous MRI study. According to controls, they had no hydrocephalus and were referred to undergo MRI for other neurological causes. CSF flowmetry was added to their study after obtaining oral informed consent from their parents.

Exclusion criteria of patients and controls were subjects older than 18 years, contraindications to MRI examination as any metallic prosthesis as cochlear implants, metallic foreign bodies, patients with ventriculoperitoneal shunts to avert any fallacy in measurements caused by the shunt, or claustrophobic or un-cooperative children having behavioral and mental disorders.

All included individuals were subjected to MRI

1.5 Tesla GE (General Electric) machine (closed magnet) with a standard head coil was used to perform all MRI scans.

Data collection

- Full history: personal history, onset, course, and duration of current illness and presenting complaints as headache, nausea, vomiting, blurring of vision and increased muscle tone, past history of trauma, intracranial hemorrhage, CNS infection, or previous operations, and family history of any CNS anomalies.
- Check of all previous radiological examination or investigations.

Clinical examination

By neurosurgeon at neurosurgery department.

Patient preparation

Any metals such as hair pins or ear rings were removed from all the participants. After reassurance of the cooperative subjects, they were informed about the procedure and examination time and inquired to stay motionless. Children younger than age 6–8 years and older children with behavioral problems (30 patients) who were not able to maintain stationary position on the MRI table throughout the whole procedure time were referred to an attending anesthesiologists who were

been responsible for administration of sedative and any required preparation.

Patient position

Neutral supine position.

MRI protocol

The MRI protocol parameters are illustrated in Table 1. In phase-contrast MRI, cardiac gating was performed with MR compatible electrodes, for detection of CSF during systole and diastole. Also, encoding velocity varied according to expected velocity in each patient. Axial images were acquired in an oblique axial plane perpendicular to the supposed direction of CSF flow at the level of aqueduct of Sylvius.

CSF flow is pulsatile and synchronous with the cardiac cycle. So, during CSF diastole, CSF moved in caudocranial direction (positive velocity) and appeared bright, whereas during CSF systole, CSF moved in the craniocaudal direction (negative velocity) which appeared dark.

Image analysis

The MR images of patients and control subjects were analyzed by two radiologists with 20 and 11 years of MRI experience, blinded to the clinical data and laboratory indicators, in a standard clinical Picture Archiving and Diagnostic System workstation, and final decisions reached by consensus are reported.

The images of cMRI were reviewed to estimate signs of hydrocephalus and underlying cause. 3D-DRIVE images were reviewed for the presence of CSF flow void sign along the aqueduct of Sylvius.

According to PC-MR images, the sagittal images were used for qualitative assessment for abnormal patterns of flow such as attenuated flow, signal inhomogeneity, and simultaneous bidirectional flow, and the axial images were used for quantitative measurements of CSF flow using the following parameters: peak systolic velocity (PSV) cm/s, peak diastolic velocity (PDV) cm/s, mean velocity (MV) cm/s, mean systolic flow (MSF) m/s, and stroke volume (SV) micro liter (μL).

In the 6 patients with arachnoid cyst, cine PC-MR and SSPS were assessed for communication of cysts with the subarachnoid spaces by noting the jet flow between the cyst and the cisterns on both sequences.

Statistical analysis

Data were coded and entered using the SPSS (Statistical Package for Social Sciences) version 20 for Windows® (IBM SPSS Inc, Chicago, IL, USA). Data were tested for normal distribution using the Shapiro–Wilk test. Qualitative data were as frequencies (count) and relative

Table 1 The parameters of MRI protocol

Sequences	Parameters
Routine MRI sequences:	TR/TE 400–600/15–25
Multiplanar T1WFSE	NEX 2 FA1/10 FOV 240 mm Matrix 224 × 384
Multiplanar T2WFSE	TR/TE 5000/105 NEX 2 FA 1/10 FOV 240 mm Matrix 224 × 384
Axial FLAIR WIS	TR/TE 11,000/140 TI 2800 ms
Axial DWI	TR/TE 3700/108
Mid sagittal steady-state free precession (SSFP) sequence	Thin cuts (3D-DRIVE) (for better assessment of CSF flow void sign along aqueduct of Sylvius)
Two-dimensional cine phase-contrast MRI sequence (2D cine PCMRI); Sagittal and axial images	Cardiac gating Flip angle: 10° TR/TE: 25/3.4 Section thickness: 1 mm Field of view: 180 mm Matrix size: 128 × 512 Encoding velocity: 5–20 cm/s encoding direction: cranio-caudal or caudo-cranial

frequencies (percentages). For comparing categorical data, chi-square test (χ^2) was used. Quantitative data were presented as mean ± SD (standard deviation) and range. For comparing between two independent groups of normally distributed variables (parametric data), Student's t test (t) was used. Probability (P value): P value less than 0.05 was considered statistically significant.

Results

This prospective study included 2 groups: a control group of 20 individuals with no hydrocephalus; 12 males (60%) and 8 females (40%) with their ages ranged from 4 to 12 years with a mean of 6.7 ± 2.584, and a patients' group including 50 patients with ventriculomegaly; 34 of them were males (68%) and 16 were females (32%) ($\chi^2 = 0.203$, $p = 0.652$) with their ages ranged from 1 to 12 years with a mean of 5.080 ± 3.303 ($t = -1.386$, $p = 0.175$).

In the control group, there were no findings consistent with hydrocephalus by cMRI. Qualitative assessment of cine PCMRI revealed average CSF flow through the aqueduct of Sylvius on systole and diastole depending on the direction of the velocity encoding; systolic CSF flow in a caudal direction appears dark and diastolic flow in a cranial direction appears bright.

Regarding to quantitative assessment of cine PCMRI in control group, velocity and flow parameters were obtained; peak diastolic velocity (PDV) ranged from 2.92 to 6.03 cm/s, peak systolic velocity (PSV) ranged from 2.7 to 6 cm/s, mean velocity (MV) ranged from 2 to 4.45 cm/s, mean systolic flow (MSF) ranged from 0.03 to 0.06 m/s and stroke volume (SV) ranged from 15 to 33 µl.

In the patients group, regarding to the final diagnosis of the studied patients reached after analysis of both cMRI and cine PCMRI of each patients and after correlation with the previous MRI studies as well as clinical correlation, there were 20 patients with aqueductal stenosis (40%), 8 patients with communicating hydrocephalus (16%), 6 patients with atrophy (12%), 6 patients with Arnold–Chiari malformation (12%), 3 patient with obstruction at foramen of Monro (unilateral obstruction (2%) and another bilateral obstruction (4%)), and 6 patients with arachnoid cysts; one was lateral ventricular arachnoid cyst (2%), 1 was suprasellar arachnoid cyst (2%), and 4 were retrocerebellar arachnoid cysts (8%), and 1 patient with Dandy–Walker variant (2%).

The positive findings of cMRI after analysis of all the studies in patients group are summarized in Table 2.

As regards quantitative assessment of cine PCMRI in patients group, velocity and flow parameters were calculated in each patient as follows:

In 20 patients of aqueductal stenosis, T2 DRIVE images revealed absent T2 flow void at aqueduct of Sylvius with thin membrane seen in 4 patients, synechiae in 6 patients, and tectal plate glioma in 1 patient, and sagittal phase images revealed absent CSF flow through the aqueduct of Sylvius on systole and diastole. No flow was detected by cine PCMRI through the aqueduct of Sylvius, and the mean values of all velocities parameters were significantly lower than those of the control group; peak diastolic velocity (PDV) ranged from 0.8 to 1.2 cm/s ($p < 0.001$), peak systolic velocity (PSV) ranged from 0.6 to 1 cm/s ($p < 0.001$), and mean velocity (MV) ranged from 0.6 to 1 cm/s ($p < 0.001$) as shown in Table 3 and Fig. 1.

In 8 patients with communicating hydrocephalus, T2 DRIVE images revealed patent aqueduct of Sylvius excluding obstruction, and sagittal phase images revealed

Table 2 Conventional MRI findings in the patients group

Diagnosis	Conventional MR findings
Aqueductal stenosis	Triventricular dilatation
Communicating hydrocephalus	Tetraventricular dilation
Brain atrophy	Prominent central and peripheral CSF spaces
Arnold–Chiari malformation	Triventricular dilatation Caudal cerebellar tonsillar herniation through foramen magnum
Dandy–Walker variant	Mild ventricular dilatation. Hypoplastic vermis Cystic dilatation of posterior fossa
Bilateral foramen of Monro obstruction	Colloid cyst seen at the site of foramen of Monro Dilation of both lateral ventricles
Unilateral foramen of Monro obstruction	Asymmetry of both lateral ventricles being larger on the right side
Lateral ventricular cyst	Mild ventricular dilation Large cyst occupying body of lateral ventricle
Retrocerebellar arachnoid cyst	Posterior fossa cystic malformation Mild dilation of supra ventricular system
Suprasellar arachnoid cyst	Large cyst occupying suprasellar cistern, compressing the third ventricle with mild dilatation of both lateral ventricles

Table 3 Comparison between control group and aqueductal stenosis, communicating hydrocephalus, brain atrophy, Dandy–Walker variant, and Arnold–Chiari malformation patients regarding velocity and flow parameters

	Diagnosis					
	Aqueduct stenosis	**Communicating hydrocephalus**	**Atrophy**	**Dandy–Walker variant**	**Arnold–Chiari malformation**	**Control**
PDV (cm/s)						
Range	0.8–1.2	7.9–11	1.1–6.03	0.8	0.9–1.3	2.92–6.03
Mean ± SD	0.97 ± 0.142	9.233 ± 1.595	1.5 ± 1.156	0.8	1.033 ± 0.231	4.428 ± 1.156
T	− 9.389	5.853	− 4.212	− 2.992	− 4.910	
P value	< 0.001*	< 0.001*	0.001*	< 0.015*	< 0.001*	
PSV (cm/s)						
Range	0.6–1	7.5–9	0.8–6	1.45	1.2–1.4	2.7–6
Mean ± SD	0.86 ± 0.165	8.1 ± 0.794	1.4 ± 1.076	1.45	1.267 ± 0.115	4.56 ± 1.076
T	− 10.747	5.218	− 4.808	− 2.755	− 5.133	
P value	< 0.001*	< 0.001*	0.001*	< 0.022*	< 0.001*	
MV (cm/s)						
Range	0.6–1	7.85–10.1	1–4.45	1.1	1.05–1.35	2–4.45
Mean ± SD	0.875 ± 0.134	8.683 ± 1.233	1.3 ± 0.782	1.1	1.150 ± 0.173	3.493 ± 0.782
T	− 10.438	8.948	− 4.636	− 2.919	− 5.006	
P value	< 0.001*	< 0.001*	0.001*	< 0.017*	< 0.001*	
MSF (m/s)						
Range	–	0.1–0.2	0.02–0.06	–	0.02–0.03	0.03–0.06
Mean ± SD	–	0.15 ± 0.05	0.027 ± 0.011	–	0.023 ± 0.006	0.049 ± 0.011
T	–	6.521	− 3.055	–	− 3.802	
P value	–	< 0.001*	0.011*	–	0.003*	
SV (μL)						
Range	–	44.6–80	5–8	–	5–9	15–33
Mean ± SD	–	61.53 ± 17.75	6.667 ± 1.528	–	6.333 ± 2.309	21.475 ± 5.898
T	–	6.572	− 4.186	–	− 4.240	
P value	–	< 0.001*	0.002*	–	0.001*	

T = Student's *t* test

p value: probability for independent samples *t* test for association between patients and control group

*Significant $p < 0.05$

prominent CSF flow through the aqueduct of Sylvius on systole and diastole. Hyperdynamic flow was detected by cine PCMRI through the aqueduct of Sylvius, and the mean values of all flow and velocity parameters were significantly higher than those of the control group; peak diastolic velocity (PDV) ranged from 7.9 to 11 cm/s ($p < 0.001$), peak systolic velocity (PSV) ranged from 7.5 to 9 cm/s ($p < 0.001$), mean velocity (MV) ranged from 7.85 to 10.1 cm/s ($p < 0.001$), mean systolic flow (MSF) ranged from 0.1 to 0.2 m/s ($p < 0.001$), and stroke volume (SV) ranged from 44.6 to 80 μl ($p < 0.001$) as shown in Table 3.

In 6 patients with brain atrophy, T2 DRIVE images revealed patent normal aqueduct of Sylvius excluding obstruction, and sagittal phase images revealed low CSF flow through the aqueduct of Sylvius on systole and diastole. Hypodynamic flow was detected by cine PCMRI through the aqueduct of Sylvius, and the mean values of all flow and velocity parameters were significantly lower than those of the control group; peak diastolic velocity (PDV) ranged from 1.1 to 6.03 cm/s (p value 0.001), peak systolic velocity (PSV) ranged from 0.8 to 6 cm/s (p value 0.001), mean velocity (MV) ranged from 1 to 4.45 cm/s (p value 0.001), mean systolic flow (MSF) ranged from 0.02 to 0.06 m/s (p value 0.011), and stroke volume (SV) ranged from 5 to 8 μl ($p < 0.002$) as shown in Table 3.

In 6 patients with Arnold–Chiari malformation, T2 DRIVE images revealed narrow aqueduct of Sylvius, and sagittal phase images revealed impaired CSF flow through the aqueduct of Sylvius on systole and diastole and no flow through posterior subarachnoid spaces with diminished flow in 4 patients and normal flow in 2 patients at the ventral subarachnoid spaces at the level of foramen magnum. Hypodynamic flow was detected

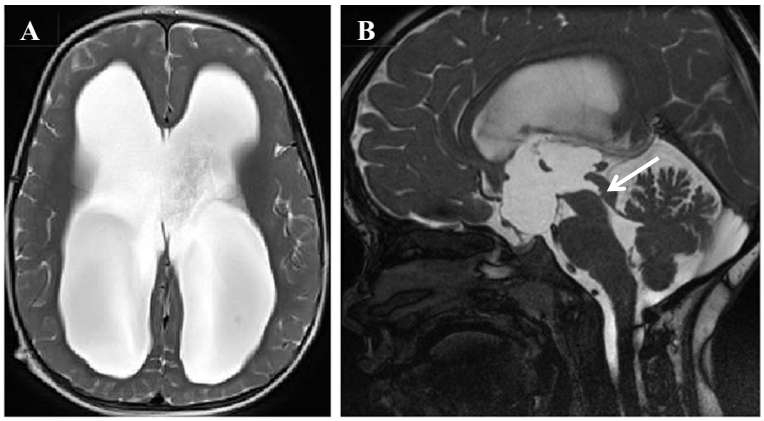

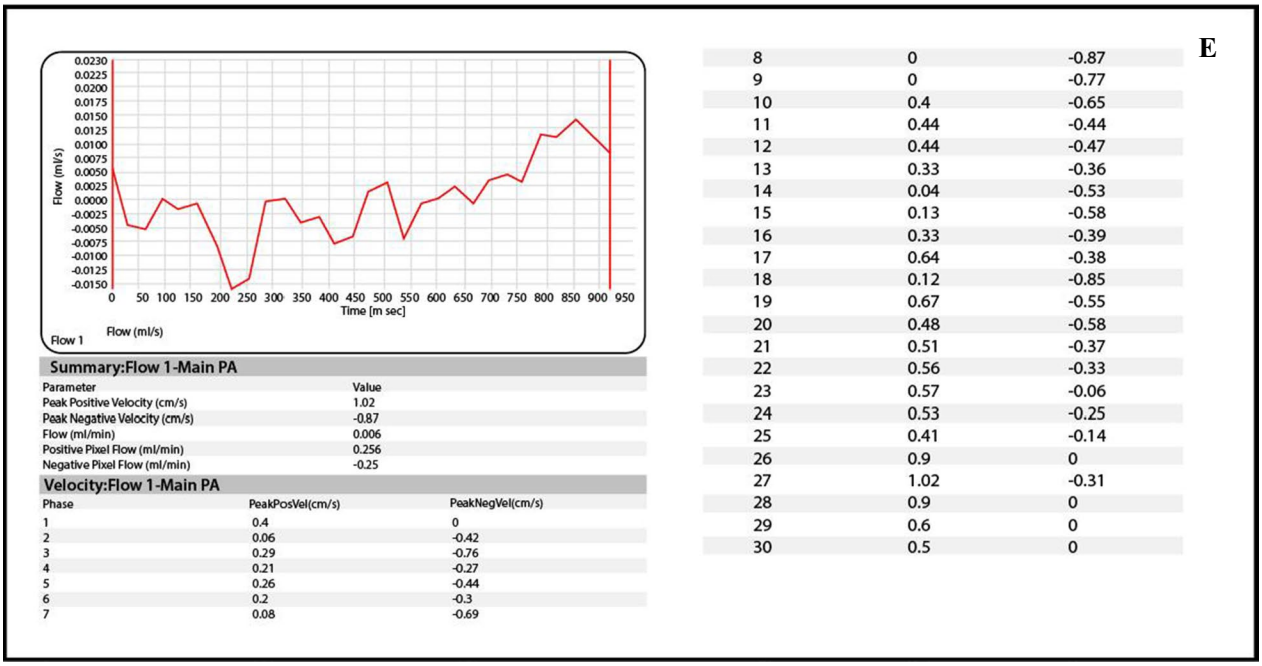

Summary:Flow 1-Main PA

Parameter	Value
Peak Positive Velocity (cm/s)	1.02
Peak Negative Velocity (cm/s)	-0.87
Flow (ml/min)	0.006
Positive Pixel Flow (ml/min)	0.256
Negative Pixel Flow (ml/min)	-0.25

Velocity:Flow 1-Main PA

Phase	PeakPosVel(cm/s)	PeakNegVel(cm/s)
1	0.4	0
2	0.06	-0.42
3	0.29	-0.76
4	0.21	-0.27
5	0.26	-0.44
6	0.2	-0.3
7	0.08	-0.69
8	0	-0.87
9	0	-0.77
10	0.4	-0.65
11	0.44	-0.44
12	0.44	-0.47
13	0.33	-0.36
14	0.04	-0.53
15	0.13	-0.58
16	0.33	-0.39
17	0.64	-0.38
18	0.12	-0.85
19	0.67	-0.55
20	0.48	-0.58
21	0.51	-0.37
22	0.56	-0.33
23	0.57	-0.06
24	0.53	-0.25
25	0.41	-0.14
26	0.9	0
27	1.02	-0.31
28	0.9	0
29	0.6	0
30	0.5	0

Fig. 1 **A**–**E** A 6-year-old female child with headache and persistent vomiting. **A** Axial T2W image shows mild-to-moderate supratentorial ventricular dilation, **B** sagittal T2 DIVER image reveals absent flow void at aqueduct of Sylvius which is obstructed by aqueductal web (white arrow). **C**, **D** Sagittal phase-contrast images reveal no CSF flow through the aqueduct at systole (**C**) and diastole (**D**) (black arrows), and **E** velocity time curve- and CSF flow curve-associated table reveals irregular CSF flow curve indicating irregular to and fro movement of the CSF proximal to the site of obstruction with PSV: 0.8 cm/s, PDV:1.02 cm/s, and MV: 0.4 cm/s (hypodynamic CSF circulation with low CSF velocities and no flow through aqueduct of Sylvius obstructive hydrocephalus due to aqueductal web)

by cine PCMRI through the aqueduct of Sylvius, and the mean values of all flow and velocity parameters were significantly lower than those of the control group; peak diastolic velocity (PDV) ranged from 0.9 to 1.3 cm/s ($p < 0.001$), peak systolic velocity (PSV) ranged from 1.2 to 1.4 cm/s ($p < 0.001$), mean velocity (MV) ranged from 1.05 to 1.35 cm/s ($p < 0.001$), mean systolic flow (MSF) ranged from 0.02 to 0.03 m/s (p value 0.003), and stroke volume (SV) ranged from 5 to 9 µl (p value 0.001) as shown in Table 3 and Fig. 2.

In 1 patient with Dandy–Walker, T2 DRIVE images revealed narrow aqueduct of Sylvius, and sagittal phase images revealed no CSF flow through the aqueduct of Sylvius on systole and diastole. No flow was detected by cine PCMRI through the aqueduct of Sylvius, and the mean values of all flow and velocity parameters were significantly lower than those of the control group; peak diastolic velocity (PDV) = 0.8 cm/s ($p < 0.015$), peak systolic velocity (PSV) = 1.45 cm/s ($p < 0.022$), and mean velocity (MV) = 1.1 cm/s ($p < 0.017$) as shown in Table 3.

According to obstructive hydrocephalus at the level of foramen of Monro, 2 patients had bilateral obstruction by colloid cyst**;** T2 DRIVE images revealed patent aqueduct of Sylvius, and sagittal phase images revealed low CSF flow through the aqueduct of Sylvius on systole and diastole. Hypodynamic flow was detected by cine PCMRI through the aqueduct of Sylvius, and the mean values of all flow and velocity parameters were lower than those of the control group; peak diastolic velocity (PDV) ranged from 1.7 to 1.85 cm/s (p value 0.051), peak systolic velocity (PSV) ranged from 1.8 to 1.93 cm/s (p value 0.037), mean velocity (MV) ranged from 1.6 to 1.72 cm/s (p value 0.046), mean systolic flow (MSF) ranged from 0.021 to 0.03 m/s (p value 0.134), and stroke volume (SV) ranged from 11.7 to 13.1 µl (p value 0.160) as shown in Table 4.

The other patient had unilateral obstruction at the level of foramen of Monro by thin membrane, T2 DRIVE images revealed patent aqueduct of Sylvius, and sagittal phase images revealed prominent CSF flow through the aqueduct of Sylvius on systole and diastole. Hyperdynamic flow was detected by cine PCMRI through the aqueduct of Sylvius, and the mean values of all flow and velocity parameters were lower than those of the control group; peak diastolic velocity (PDV) = 7.9 cm/s ($p < 0.019$), peak systolic velocity (PSV) = 7.8 cm/s ($p < 0.018$), mean velocity (MV) = 7.85 cm/s ($p < 0.001$), mean systolic flow (MSF) = 0.18 m/s ($p < 0.001$), and stroke volume (SV) = 61 µl ($p < 0.001$) as shown in Table 4 and Fig. 3.

In 6 patients with arachnoid cysts; lateral ventricular, retrocerebellar and suprasellar cysts, T2 DRIVE images revealed patent normal aqueduct of Sylvius excluding obstruction, and sagittal phase images revealed average CSF flow through the aqueduct of Sylvius on systole and diastole. Normal dynamic flow was detected by cine PCMRI through the aqueduct of Sylvius, and the mean values of all flow and velocity parameters were within normal as those of the control group. Phase-contrast images revealed no jet flow between the investigated cysts and neighboring subarachnoid spaces and cisterns (Fig. 4).

Discussion

Different types of neurological diseases cause abnormality in CSF dynamics with subsequent development of many neurological symptoms and signs. Evaluation of cerebrospinal fluid (CSF) was based fundamentally on invasive procedures such as lumbar puncture, myelographies, radioisotope studies, or intracranial pressure monitoring that gave important information about CSF abnormalities in different CNS disorders [3, 8].

So, those examinations were considered the cornerstone for most of the basics of CSF physiology and pathophysiology. Nowadays, remarkable evolution of imaging techniques has provided noninvasive modalities for flow assessment, e.g., phase-contrast magnetic resonance imaging (PCMRI) that facilitates qualitative and quantitative evaluation of CSF flow [8].

This study included 50 patients in whom the diagnosis of hydrocephalus was established. There were 34 males and 16 females with age range of 1–12 years. A control matched age group of 20 subjects who did not suffer from hydrocephalus was also included. This control group was assessed qualitatively and quantitatively by phase-contrast MRI to provide normal reference values for comparison.

Aqueduct of Sylvius is the main of obstruction as a result of its narrow caliber. This can be secondary to congenital stenosis, web or acquired either due to post-inflammatory adhesions or external compression [9, 10].

3D-DRIVE can accurately demonstrate the obstructed/stenosed aqueduct and describe its shape (either tubular narrowing, focal obstruction/stenosis, associating proximal funneling) [9, 11].

When T2 flow void is absent on sagittal T2 images (3D-DRIVE), it is as a complementary sign of obstruction of aqueduct, but not a reliable sign because the intensity of flow void is affected by different factors as diameter of aqueduct, velocity of CSF, and section thickness through PCMRI. If the aqueduct is physiologically narrow, but not stenosed, this sign may be absent or weak [7, 12, 13].

In the present study, all the 20 patients with suspected aqueductal stenosis showed supraventricular dilatation, all of them showed absence of flow void at aqueduct of Sylvius and quantitative assessment showed

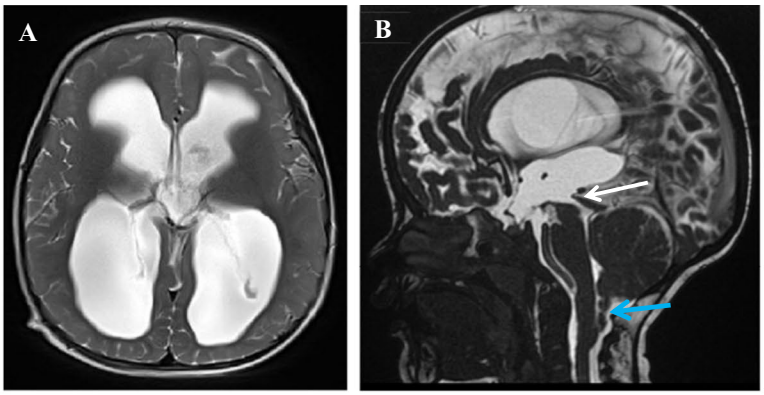

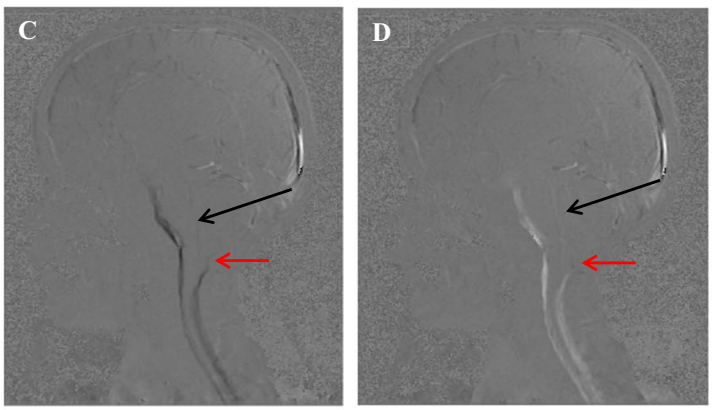

E

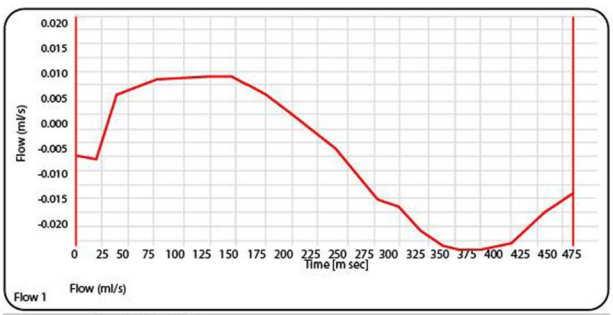

Summary:Flow 1-Main PA	
Parameter	Value
Peak Positive Velocity (cm/s)	0.95
Peak Negative Velocity (cm/s)	-1.22
Flow (ml/min)	-0.405
Positive Pixel Flow (ml/min)	0.179
Negative Pixel Flow (ml/min)	-0.584

Velocity:Flow 1-Main PA		
Phase	PeakPosVel(cm/s)	PeakNegVel(cm/s)
1	0.05	-0.56
2	0	-0.54
3	0.57	-0.13
4	0.76	-0.24
5	0.9	-0.17
6	0.95	-0.22
7	0.93	-0.14
8	0.9	-0.17
9	0.78	-0.17
10	0.64	-0.23
11	0.39	-0.25
12	0.18	-0.34
13	0.13	-0.42
14	0.11	-0.59
15	0	-0.82
16	0.04	-0.94
17	0	-1.07
18	0	-1.11
19	0	-1.22
20	0	-1.14
21	0	-1.06
22	0	-1.01
23	0	-0.95
24	0.03	-0.87

Fig. 2 **A**–**E** A 5-year-old male child with headache and blurred vision. **A** Axial T2W image shows moderate dilatation of supratentorial ventricles, **B** sagittal T2 DIVER image reveals caudal cerebellar tonsil herniation through foramen magnum (blue arrow), peaked tectum (white arrow), and narrowing of cerebral aqueduct of Sylvius, **C**, **D** sagittal phase-contrast images reveal low CSF flow through the aqueduct at systole (**C**) and diastole (**D**) (black arrows), no CSF flow at posterior subarachnoid space (red arrows), and **E** velocity time curve- and CSF flow curve-associated table reveals CSF in both diastole (above the base line) and systole (below the base line) with PSV: 1.2 cm/s, PDV: 0.9 cm/s, MV: 1.05 cm/s, MSF: 0.02 m/s, and SV: 5 µl (hypodynamic CSF circulation with low CSF velocities and stroke volume at aqueduct of Sylvius and no CSF flow at posterior subarachnoid space at the level of foramen magnum Arnold–Chiari malformation)

Table 4 Comparison between control group and patients with obstruction at the level of foramen of Monro regarding velocity and flow parameters

	Diagnosis		
	Unilateral obstruction at foramen of Monro	**Bilateral obstruction at foramen of Monro**	**Control**
PDV (cm/s)			
Range	7.9	1.7–1.85	2.92–6.03
Mean ± *SD*	7.9	1.775 ± 0.106	4.428 ± 1.156
T	2.864	− 2.250	
P value	< 0.019*	0.051*	
PSV (cm/s)			
Range	7.8	1.8–1.93	2.7–6
Mean ± *SD*	7.8	1.856 ± 0.091	4.560 ± 1.076
T	2.870	-2.445	
P value	< 0.018*	0.037*	
MV (cm/s)			
Range	7.85	1.6–1.72	2–4.45
Mean ± *SD*	7.85	1.66 ± 0.044	3.493 ± 0.782
T	5.314	− 2.309	
P value	< 0.001*	0.046*	
MSF (m/s)			
Range	0.18	0.021–0.03	0.03–0.06
Mean ± *SD*	0.18	0.025 ± 0.006	0.049 ± 0.011
T	11.350	− 1.646	
P value	< 0.001*	0.134	
SV (µL)			
Range	61	11.7–13.1	15–33
Mean ± *SD*	61	12.4 ± 0.989	21.475 ± 5.898
T	6.390	− 1.532	
P value	< 0.001*	0.160	

T = Student's *t* test

p value: probability for independent samples *t* test for association between patients and control group

*Significant $p < 0.05$

hypodynamic flow through the aqueduct, with lower velocity parameters compared to normal parameters of healthy subjects of the control group.

These findings were consistent with those of Abdelhameed et al. [4], Parkkola et al. [5], and Lucic et al. [14] who diagnosed aqueductal stenosis in their studies by cMRI findings, and by hypodynamic flow through aqueduct of Sylvius on phase-contrast images.

Regarding diagnosis of communicating hydrocephalus, it is often suggested by the presence of tetraventricular dilatation on conventional MR images and increased T2 flow void (3DRIVE) and confirmed by the presence of hyperdynamic CSF flow at the aqueduct of Sylvius on phase-contrast MRI [5, 10].

Eight patients with communicating hydrocephalus were evaluated in our study and CSF flowmetry revealed significant increased CSF flow and velocities through aqueduct of Sylvius.

These results match with those of Abdelhameed et al. [4] and Lucic et al. [14], who performed a study on patients with communicating hydrocephalus. The CSF flow velocity through aqueduct was significantly higher than that of the control groups. This is attributed to reduced arterial compliance, causing increased capillary pulse pressure and brain parenchymal expansion that is directed inwards toward the ventricular system causing increased intraventricular pulse pressure and elevated aqueductal systolic CSF flow.

In many patients, cortical cerebral atrophy is associated with ventricular dilatation, and conventional MRI has a limited role in portending whether this ventriculomegaly is a compensatory enlargement due to reduced brain parenchymal volume or caused by an actual pathology causing hydrocephalus. So, phase-contrast MRI is needed as a complementary technique to reach an accurate diagnosis of the cause of ventriculomegaly [16].

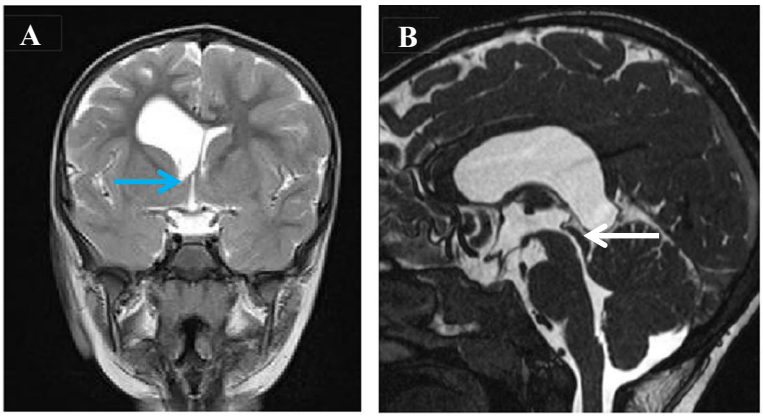

E

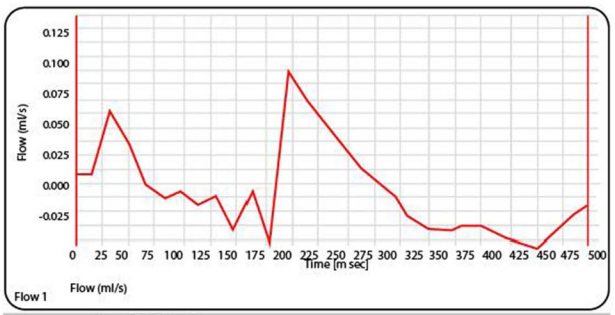

Summary:Flow 1-Main PA

Parameter	Value
Peak Positive Velocity (cm/s)	7.94
Peak Negative Velocity (cm/s)	-7.81
Flow (ml/min)	-0.133
Positive Pixel Flow (ml/min)	1.176
Negative Pixel Flow (ml/min)	-1.31

Velocity:Flow 1-Main PA

Phase	PeakPosVel(cm/s)	PeakNegVel(cm/s)
1	1.1	0
2	1.1	0
3	5	0
4	6.47	-5.57
5	1.72	-3.09
6	0.83	-1.46
7	0.73	-0.92
8	0.2	-2.16
9	7.94	-4.6
10	7.94	-6.52
11	7.8	-5.43
12	6.7	-7.81
13	4.8	0
14	3.6	0
15	2.9	0
16	2.45	0
17	1.99	-0.07
18	1.05	-0.61
19	0	-1.6
20	0	-2.34
21	0	-2.77
22	0	-2.62
23	0	-2.13
24	0	-2.09
25	0	-2.4
26	0	-2.97
27	0	-3.57
28	0	-2.54
29	0	-1.55
30	0	-1.03

Fig. 3 **A**–**E** A 10-year-old male child with headache and blurring of vision. **A** Coronal T2W image shows asymmetry of both lateral ventricles being larger on the right side with obstructing membrane in the right foramen of Monro (blue arrow), **B** sagittal T2 DIVER image reveals patent normal aqueduct (white arrow), **C**, **D** axial phase-contrast images reveal normal CSF flow through the aqueduct at systole (**C**) and diastole (**D**) (black arrows), and **E** velocity time curve- and CSF flow curve-associated table reveals irregular CSF flow curve indicating irregular to and fro movement of the CSF proximal to the site of obstruction with PSV: 7.8 cm/s, PDV:7.9 cm/s, MV: 7.8 cm/s, MSF: 0.176 m/s and SV: 61 µl (hyperdynamic CSF circulation with high CSF velocities and stroke volume and normal flow through aqueduct of Sylvius unilateral obstructive hydrocephalus at level of foramen of Monro by a membrane)

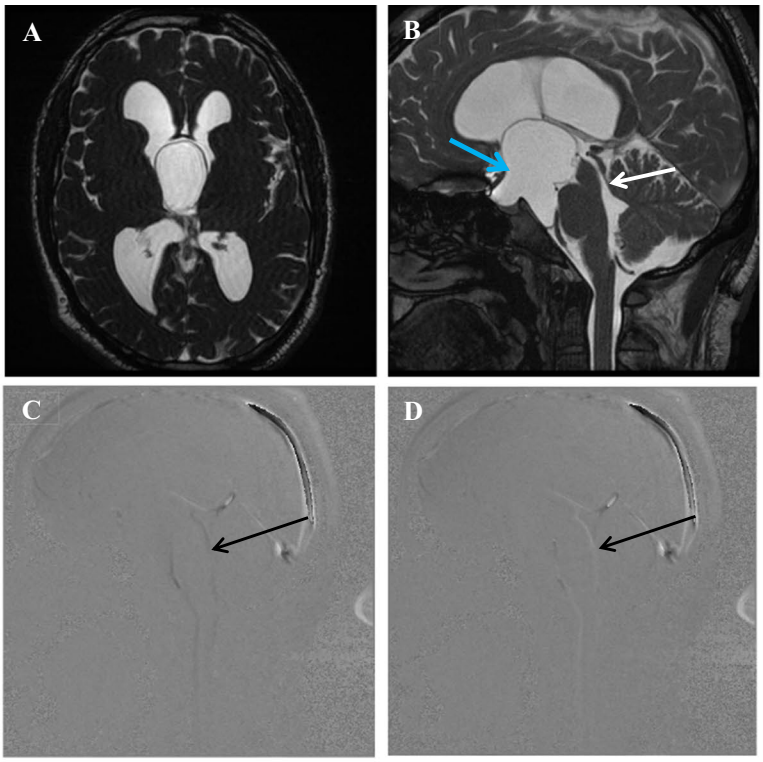

E

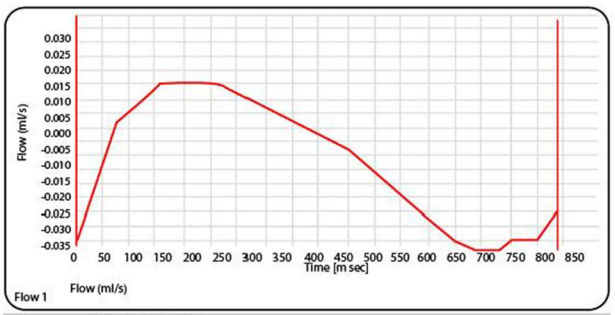

Summary:Flow 1-Main PA

Parameter	Value
Peak Positive Velocity (cm/s)	2.92
Peak Negative Velocity (cm/s)	-5.98
Flow (ml/min)	-0.534
Positive Pixel Flow (ml/min)	0.259
Negative Pixel Flow (ml/min)	-0.793

Velocity:Flow 1-Main PA

Phase	PeakPosVel(cm/s)	PeakNegVel(cm/s)
1	0	-2.92
2	0	-1.62
3	0.6	0
4	1.5	0
5	2.4	0
6	2.9	0
7	2.9	0
8	2.5	0
9	2.1	0
10	1.6	0
11	1.1	0
12	0.6	0
13	0.03	-0.23
14	0	-0.96
15	0	-2.1
16	0	-3.24
17	0	-4.47
18	0	-5.4
19	0	-5.89
20	0	-5.98
21	0	-5.82
22	0	-5.36
23	0	-4.91
24	0	-3.85

Fig. 4 **A**–**E** A 10-year-old male child with headache and blurred vision. **A** Axial FIESTA image shows mild dilation of supratentorial ventricular system, and cystic lesion at floor of third ventricle. **B** Sagittal T2 DIVER image reveals patent normal aqueduct with normal flow void (white arrow) and a suprasellar cystic lesion (blue arrow) reaching the floor of third ventricle and compressing it with no communication between the cyst and neighboring CSF spaces. **C**, **D** Sagittal phase-contrast images reveal normal CSF flow through the aqueduct at systole (**C**) and diastole (**D**) (black arrows) with no jet flow between intra ventricular cyst lesion and neighboring CSF spaces, and **E** velocity time curve- and CSF flow curve-associated table reveals CSF in both diastole (above the base line) and systole (below the base line) with PSV: 5.9 cm/s, PDV:2.92 cm/s, MV: 4.45 cm/s, MSF: 0.04 m/s and SV: 16.6 µl (normal dynamic CSF circulation with normal CSF velocities and stroke volume and normal flow through aqueduct of Sylvius obstructive hydrocephalus due to compression of the third ventricle by a suprasellar arachnoid cyst not communicating with CSF spaces)

The present study included 6 patients presenting with various symptoms including global developmental delay, vomiting, and decreased IQ. Ventriculomegaly and cortical brain atrophy were observed on conventional MR images.

On phase-contrast MRI, the patients with cerebral atrophy in this study had positive flow through the aqueduct of Sylvius. Quantitatively, there was a significant decrease in all flow and velocity parameters through the aqueduct of Sylvius compared to those of the control group. The decreasing flow of CSF through the aqueduct is due to reduction in brain parenchymal size in case of cerebral atrophy that leads to decreased compression on ventricular system [16].

Al-Haggar et al. [17] and Abdalla et al. [18] also found a drop in all parameters in brain atrophy group in comparison with control group indicating hypodynamic CSF flow. So, PCMRI is validated tool in distinguishing cases of communicating hydrocephalus and brain atrophy.

Patients with Chiari malformation type I may have abnormalities in CSF dynamics that do not correlate with the degree of morphologic abnormality seen on anatomical imaging studies. These abnormalities can be reached by phase-contrast MRI helping in both diagnosis of Chiari malformation type I and in guiding surgical intervention [19, 20].

In our study, 6 patients with Chiari malformation were evaluated for their CSF flow patterns at the aqueduct of Sylvius and the foramen magnum. No flow was detected in the posterior cervical subarachnoid space qualitatively, with diminished flow (4 patients) and normal flow (2 patients) in the ventral subarachnoid space and diminished flow at aqueduct of Sylvius. Similarly, Abdelhameed et al. [4] performed a study on 2 patients with Chiari I malformation and found significant difference in quantitative assessment of CSF velocities in comparison with the normal volunteers. One of them showed positive CSF flow at both foramen Magnum and aqueduct of Sylvius, and in the other patient, no flow was detected in the posterior cervical subarachnoid space as well as in the aqueduct of Sylvius.

Contrary to our study, Wang et al. [20] and Al-Haggar et al. [17] found a significant increase in PSV and PDV in Chiari malformation type I patients. This difference in CSF pattern in Chiari patient is attributed to the difference of age of presentation.

In Dandy–Walker malformations, it is difficult to identify wall of the cyst by MRI to distinct between DWM and arachnoid cysts in the posterior fossa, and the differentiation depends on the absence of a communication of displaced 4th ventricle with the cystic extra-axial area in case of arachnoid cysts [21, 22].

Flow-sensitive MRI techniques and three-dimensional high-resolution sequences have provided functional and anatomical assessment of CSF flow dynamics, respectively. For DWM, the determination of CSF flow changes is mandatory for the differential diagnosis, and for the indication of the treatment for the hydrocephalus. In the classic DWM, the phase-contrast study demonstrates no flow between the posterior fossa cystic space and the posterior fossa cervical subarachnoid space [23].

Our study included only one patient with cystic dilatation of the posterior fossa. The patient showed hypoplasia of cerebellar vermis and Blake's pouch cyst on conventional MR images and aqueduct stenosis with hypodynamic flow of CSF circulation by quantitative assessment and no communication between the cyst and the posterior cervical subarachnoid space on cine images, as reported by Mohammad et al. [24] and Yildiz et al. [25].

Contrary to our study, Abdelhameed et al. [4] and Mohanty et al. [22] reported that their patients showed positive CSF flow at the aqueduct of Sylvius on cine images, with normal parameters in quantitative assessment. The discrepancy in the results may be attributed to the small sample size in our study and that of Yildiz et al. [25] which included only 2 patients with DWV. A larger sample size may be required to establish the pattern of CSF dynamics in DWV patients.

Idiopathic foramen of Monro closure or narrowing by membranous occlusion is a rare event that usually occurs in children or infants, and only few cases are reported about it in the literature [26].

This study included one patient with unilateral right ventricular dilatation. The patient underwent phase-contrast MRI, which revealed hyperdynamic CSF circulation quantitatively and patent aqueduct of Sylvius by qualitative assessment, thus eliminating any suspected doubt of obstruction at those sites. Since the patient had unilateral ventricular dilatation, the diagnosis of foramen of Monro obstruction was suspected and was confirmed by observation of membranous obstruction on T2 DRIVE images. Boruah et al. [27] reported 3 cases in their study with unilateral hydrocephalus, also, Abdelhameed et al. [4] reported 1 case in their study with unilateral hydrocephalus, those cases had normal flow at aqueduct of Sylvius and foramen magnum, and were eventually diagnosed with unilateral foramen of Monro obstruction.

According to arachnoid cysts, they are lesions filled with cerebrospinal fluid (CSF) lined by the arachnoid membrane. Typically, arachnoid cysts are not associated with hydrocephalus, but may cause a mass effect according to size and location. A phase-contrast study can demonstrate whether the cyst is communicating to the CSF spaces, which is important in preoperative planning [9, 28, 29]. In our study, none of the investigated patients

with arachnoid cysts had a communicating arachnoid cyst with subarachnoid spaces or cisterns; no pulsatile CSF flow (dark and bright signal alternation) was detected at the neck of the cysts.

Elsafty et al. [13] studied CSF flow in six persons with previously diagnosed arachnoid cyst. Two patients had communicating arachnoid cysts proved by the presence of jet flow between the cyst and the cisterns on cine PC-MR and SSPS sequence, and 4 patients had non-communicating arachnoid cysts with no alteration in signal intensity within the cyst; the results were confirmed by surgery.

Our study included several limitations: first unclear history for all patients because of parents' ignorance of the nature of children's illness. Second, our study included small number of patients in most of pathologies which was not sufficient to establish their CSF flow patterns. Third, anesthesia was required in some un-cooperative patients, which was suspected to affect the CSF flow at aqueduct causing some fallacies in the results, as reported by Parkkola et al. [5]. Fourth, during performing phase-contrast MRI, choice of ROI for quantitative assessment was not the same in all studies, which may cause discrepancies in some results, and this limitation was also reported in 2003 by Haughton et al. [30]. Finally, we had to repeat some studies several times to reach the most suitable VENC value for the patient.

Conclusions

This study realized that CSF flowmetry using phase-contrast MRI has a crucial role in discrimination of different types of hydrocephalus in pediatric patients, proper localization of site of obstruction, detection of combined pathologies through determination of alterations in CSF movement as well as changes in CSF velocities and flow parameters.

We recommend using phase-contrast MR images in all cases of hydrocephalus to reach accurate diagnosis for proper selection of the treatment strategy and improving the postoperative outcome. Also, many studies with larger sample are needed to determine variation in CSF flow pattern in different pathologies.

Abbreviations

CNS	Central nervous system
CSF	Cerebrospinal fluid
cMRI	Conventional magnetic resonance imaging
DWM	Dandy–Walker malformation
MSF	Mean systolic flow
MV	Mean velocity
PCMRI	Phase-contrast magnetic resonance imaging
PDV	Peak diastolic velocity
PSV	Peak systolic velocity
ROI	Region of interest
SSFP	Steady-state free precession
SV	Stroke volume
T1WFSE	T1-weighted fast spin-echo sequence
T2WFSE	T2-weighted fast spin-echo sequence
VENC	Velocity encoding

Acknowledgements

We acknowledge all the participants for their cooperation and patience.

Author contributions

All authors read and approved the final manuscript for submission. MF suggested the research idea, ensured the original figures and data in the work, minimized the obstacles to the team of work, correlated the study concept and design, and had the major role in analysis, GA collected data in all stages of manuscript, performed data analysis. HA supervised the study with significant contribution to design the methodology, manuscript revision, and preparation. YF correlated the clinical data of patient and matched it with the findings and drafted and revised the work. All authors read and approved the final manuscript.

Funding

No funding was obtained for this study.

Availability of data and materials

The author's confirm that all data supporting the finding of the study are available within the article and the raw data ad data supporting the findings were generated and available at the corresponding author on request.

Declarations

Ethics approval and consent to participate

Informed written consents were taken from the patients and healthy volunteers, and the study was approved by ethical committee of Tanta university hospital, faculty of medicine. Committee's reference number: 32735/11/18.

Consent for publication

All participants included in the research gave written consent to publish the data included in the study.

Competing of interest

The authors declare that they have no competing of interests.

Received: 26 September 2022 Accepted: 13 January 2023
Published online: 01 February 2023

References

1. Kahle T, Kulkarni V, Limbrick D et al (2016) Hydrocephalus in children. The Lancet 387(10020):788–799
2. Ville L, Vanninen R, Rauramaa T (2018) Cerebrospinal fluid circulation and hydrocephalus. Handb Clin Neurol Elsevier 145:39–50
3. Alves T, Ibrahim ES, Martin BA et al (2017) Principles, techniques, and clinical applications of phase-contrast magnetic resonance cerebrospinal fluid imaging. Neurographics 7(3):199–210
4. Abdelhameed AM, Darweesh AF, Bedair MH (2017) Role of MRI CSF flowmetry in evaluation of hydrocephalus in pediatric patients. Egypt J Hosp Med 68(2):1291–1296
5. Parkkola R, Komu MA, Arimaa T et al (2001) Cerebrospinal fluid flow in children with normal and dilated ventricles studied by MRI imaging. Acta Radiol 42(1):33–38
6. Mohammad SA, Osman N, Battal B et al (2018) Phase-contrast and three-dimensional driven equilibrium (3D-DRIVE) sequences in the assessment of pediatric obstructive hydrocephalus. Childs Nerv Syst 34:2223–2231
7. Algin O, Hakyemez B, Parlak M (2010) Phase-contrast MRI and 3D-CISS versus contrast-enhanced MR cisternography on the evaluation of the aqueductal stenosis. Neuroradiology 52(2):99–108
8. Korbecki A, Zimny A, Podgórski P et al (2019) Imaging of cerebrospinal fluid flow: fundamentals, techniques, and clinical applications of phase-contrast magnetic resonance imaging. Pol J Radiol 84:e240–e250

9. Stoquart S, Lehman P, Gondary C et al (2009) Phase contrast MR imaging support for the diagnosis of acqueductal stenosis. Am J Neuroradiol 30(1):209–214
10. Frassanito P, Goker B, Di Rocco C. Aqueductal stenosis and hydrocephalus. In: Textbook of pediatric neurosurgery. 2020. p. 501–19]
11. Orman G, Rossi A, Meoded A et al. Children with acute neurological emergency. In: Farb R, Rovira À (eds) Hydrocephalus and CSF disorders diseases of the brain, head and neck, spine. 2020. p. 11–24]
12. Algin O, Turkbey B (2012) Evaluation of aqueductal stenosis by 3D sampling perfection with application-optimized contrasts using different flip angle evolutions sequence: preliminary results with 3T MR imaging. Am J Neuroradiol 33(4):740–746
13. Elsafty HG, ELAggan AM, Yousef MA et al (2018) Cerebrospinal fluid flowmetry using phase-contrast MRI technique and its clinical applications. Tanta Med J 46(2):121
14. Lucic MA, Bjelan M, Koprivsek K et al. Quantitative dynamic phase-contrast MRI analysis of the CSF flow values within the stenotic and obstructed cerebral aqueduct. In: European congress radiology of ECR. 2012. p. 1–7.
15. Vivas-Buitrago T, Lokossou A, Jusué-Torres I et al (2019) Aqueductal cerebrospinal fluid stroke volume flow in a rodent model of chronic communicating hydrocephalus: establishing a homogeneous study population for cerebrospinal fluid dynamics exploration. World Neurosurg 128:e1118–e1125
16. Baker II, Elsayed N, Kalioubie MM et al (2009) Brain atrophy versus normal pressure hydrocephalus by CSF flow measurement at MRI. Med J Cairo Univ 77(1):19–26
17. Al-Haggar M, Salama D, Ahmad N (2021) MRI CSF flowmetry in evaluation of different neurological diseases. Egypt J Radiol Nuclear Med 52(1):1–10
18. Abdalla RN, Zghair MAG (2019) The role of magnetic resonance imaging cerebrospinal fluid flowmetry in differentiation between normal flow hydrocephalus and involutional brain atrophy. JPMA J Pak Med Assoc 69(8):S78–S82
19. Delavari N, Wang AC, Bapuraj JR et al (2020) Intraoperative phase contrast MRI analysis of cerebrospinal fluid velocities during posterior fossa decompression for Chiari I malformation. J Magn Reson Imaging 51(5):1463–1470
20. Wang CS, Wang X, Fu CH et al (2014) Analysis of cerebrospinal fluid flow dynamics and morphology in Chiari I malformation with cine phase-contrastmagnetic resonance imaging. Actaneurochirurgica 156(4):707–713
21. Correa GC, Amaral LF, Vendolin LM (2011) Neuroimaging of Dandy–Walker malformation-new concept. Topic Magn Reson Imaging 22(6):303–312
22. Mohanty A, Biswas A, Satish S et al (2006) Treatment options for Dandy–Walker malformation. J Neurosurg 105:348–56
23. Dastoli AD, Nicácio JM, Da Costa DS et al (2020) Hydrocephalus and Dandy-Walker malformation: a review. Arch Pediatric Neurosurg 2:e442020–e442020
24. Mohammad SA, Osman NM, Ahmed KA (2019) The value of CSF flow studies in the management of CSF disorders in children: a pictorial review. Insights Imaging 10(1):1–13
25. Yildiz H, Yazici Z, Hakyemez B et al (2006) Evaluation of CSF flow patterns of posterior cystic fossa malformations using CSF flow MR imaging. Neuroradiology 48(9):595–605
26. De Bonis P, Anile C, Tamburrini G et al (2008) Adult idiopathic occlusion of the foramina of Monro: diagnostic tools and therapy. J Neuroimaging 18(1):101–104
27. Boruah DK, Arora M, Prakash A et al (2016) Idiopathic unilateral foramen of Monro stenosis: neuroimaging findings in three patients. J Evid Based Med Health Care 3(34):1673–1675
28. Battal B, Kocaoglu M, Bulakbasi N et al (2011) Cerebrospinal fluid flow imaging by using phase-contrast MR technique. Br J Radiol 84(1004):758–765
29. Kau T, Marterer R, Kottke R et al (2020) Blake's pouch cysts and differential diagnoses in prenatal and postnatal MRI. Clin Neuroradiol 30(3):435–445
30. Haughton VM, Korosec FR, Medow JE et al (2003) Peak systolic and diastolic CSF velocity in the foramen magnum in adult patients with Chiari I malformations and in normal control participants. AJNR 24(2):169–176

Publisher's Note